ADVANCED ELECTRONIC MATERIALS
www.advelectronicmat.de

Highly Stable Forming-Free Bipolar Resistive Switching in Cu Layer Stacked Amorphous Carbon Oxide: Transition between C—C Bonding Complexes

*Da Seul Hyeon, Gabriel Jang, SunHwa Min, and Jin Pyo Hong**

Recent advances in resistive switching devices have garnered a considerable amount of interest as an alternative option for next-generation nonvolatile memories due to their distinct advantages of ultralow power consumption, fast operation, and outstanding scaling potential. Among the recently considered active media, amorphous carbon oxide (α-C:O$_x$) shows promise in terms of device performance, essentially due to the transition between carbon sp^2–sp^3 complex under bias. However, widespread utilization of this media still remains a challenge due to its undesirable high forming voltage and insufficient stability issues. Here, a simple approach to stack a suitable Cu layer at the α-C:O$_x$ layer/W interface of simple Pt/α-C:O/W frames is introduced to engineer resistive switching characteristics. Precise control of a stacked Cu layer (2.5 nm thick) identifies numerous benefits of forming-free characteristics, reliable switching time, and appreciably stable features compared with those of single α-C:O$_x$ active medium. The possible principle underlying the experimental findings is described based on the oxygen ion drift-driven transition between sp^2 and sp^3 bonds at the intermixed regions of α-C:O$_x$/Cu interfaces under bias, which are systematically confirmed by structural observations.

1. Introduction

Resistive random access memory devices based on resistive switching (RS) characteristics are gaining importance as a promising alternative for next-generation memory due to their distinctive features, including a geometrically simple frame, ultralow power consumption, high speed operation, and outstanding scaling potential.[1–6] To further ensure such features, substantial efforts have been dedicated toward developing a suitable candidate for data storage media.[7–9] In recent years, carbon-based media has shown great potential as a reliable option owing to its low cost, simple chemical composition, affordable compatibility with complementary metal-oxide-semiconductor processes, and fast switching speed.[10–13] Thus, numerous studies have also been conducted to attain a firm understanding of the nature and to achieve improved device performance.

To date, the possible underlying nature of carbon layer-based RS has been expected to the formation and rupture of existing sp^2 conductive filament (CFs) initially arising from the electroforming step: that is, the conversion between the sp^2 and sp^3 carbon complexes takes places via bias, leading to two representative RS behaviors. One class is unipolar RS frequently observed from the tetrahedral amorphous carbon (tα-C)[14,15] or diamond-like carbon (DLC) layer.[16–18] The corresponding unipolar RS is likely attributable to the fuse–antifuse process induced by the current-driven temperature increase. The second class is bipolar-RS, mainly observed in graphene oxides[19–21] or α-C:H[22] layers, where bias-dependent oxygen or hydrogen ion drift plays a crucial role in the transition between the sp^2 and sp^3 bonds through the removal or absorption of ions under bias. Recently, other promising work addressed the advancing device performance of oxygenated amorphous carbon (α-C:O$_x$) layers, such as the high on/off ratio and fast switching speed compared to graphene oxide.[21,23] Furthermore, this α-C:O$_x$ active layer is also expected to play a key role in providing simple wafer-scale fabrication allowing good reproducibility at room temperature, amorphous nature, high degree of tunable chemical characteristics by simply changing oxygen content, and outstanding device performance, compared with those of other resistive switching active layer. However, these α-C:O$_x$ layer-based devices exhibited higher forming voltages and insufficient stability/reliability features, even if they did possess an appreciable switching speed.[18,24] In addition, the stochastic distribution in forming voltages during consecutive sweeps led to significant variation in device performance, thus requiring high power consumption to address all individual cells.[25–27]

D. S. Hyeon, G. Jang, J. P. Hong
Research Institute of Natural Science
Department of Physics
Hanyang University
Seoul 133-791, South Korea
E-mail: jphong@hanyang.ac.kr

S. H. Min, J. P. Hong
Research Institute for Convergence of Basic Science
Division of Nanoscale Semiconductor Engineering
Hanyang University
Seoul 133-791, South Korea

The ORCID identification number(s) for the author(s) of this article can be found under https://doi.org/10.1002/aelm.202100660.

DOI: 10.1002/aelm.202100660

The presence of forming voltages in α-C:O_x layer-based devices may cause a possible hard-breakdown event to take places owing to the requirement of a relatively high voltage during forming operation, thereby significantly impacting adjacent devices in future integrated crossbar array frames. The above forming issue also reflects the inherent necessity of additionally separate circuits which may lead to device design burdens. The corresponding results seem to be mainly caused by uncontrollable or random rupture/creation events of sp^2 CFs initially created by the forming process. Thus, proper manipulation of sp^2–sp^3 conversion in the α-C:O_x layer becomes a key step toward extending their wide use, together with identifying the possible nature of electrical transport.

In this work, we address a simple Cu layer stacking approach to improve device performance in α-C:O_x layer-based RS devices. The initial concept of this work is the manipulation of sp^2–sp^3 bonding ratios by placing a suitable thin Cu layer into the α-C:O_x active layer/W bottom electrode interfaces, which tailors the sp^2/sp^3 bonding ratio in the intermixed regions of α-C:O_x/Cu interfaces created during device fabrication. Precise control of the stacked Cu layer thickness enhanced the device performance, including forming-free characteristics and improved reliability features. Extensive X-ray photoelectron spectroscopy (XPS) and transmission electron microscope (TEM) measurements were conducted to verify the improved device performance. Experimental observations identified efficient conversion between the sp^2 and sp^3 bonds in the intermixed region of the α-C:O_x/Cu interfaces.

2. Results and Discussion

Two sets of samples were prepared: Pt/α-C:O_x(8)/W and Pt/α-C:O_x(8)/Cu(2.5)/W. The former and latter are hereafter termed as Samples A and B, respectively, where the numbers in parentheses indicate the nominal thickness of each layer in nanometers. During operation, a bias voltage was applied to the top Pt electrode with the bottom W electrode grounded. **Figure 1**a,b plots the representative *I*–*V* responses of Samples A and B with 320 nm diameters in W bottom electrodes, respectively, exhibiting bipolar RS behaviors. It can be seen that Sample A required typical negative electroforming voltages of about −3 to −4 V as in most RS setups. Sample B contained a 2.5 nm thick Cu layer and exhibited forming-free characteristics upon applying a compliance current (I_{cc}) of 100 μA (black line). Figure S1 in the Supporting Information displays more detailed *I*–*V* characteristics of Sample A, including various oxygen contents induced by the application of different oxygen partial pressures during fabrication. As evident in the figure, Sample A with no oxygen content did not exhibit typical RS behavior, while increasing the oxygen content in the α-C:O_x layer yielded increased forming voltages (V_f). These results are likely associated with the presence of different contents in the sp^2 bonds, depending on oxygen ions, as will be explained later. As depicted above, it is widely believed that the possible RS nature of carbon or α-C:O_x layer-based devices directly relates to the contents of sp^2 bonds constituting the CF paths, which in turn leads to a low resistance state (LRS). Thus, to elucidate the influence of oxygen ion content on the performance of α-C:O_x layer-based devices, oxygen content-dependent XPS analyses were conducted by adapting various oxygen partial pressures during device fabrication (Figure S2, Supporting Information). The results suggest that the oxygen content generated by different oxygen partial pressures inversely contributes to the content of sp^2 bonds; that is, a possible reaction between the oxygen ions and sp^2 bonds establishes the conversion from sp^2 to C—C sp^3 bonds, which leads to a relatively resistive state. This means that the C—C sp^3 bonds are also converted to sp^2 bonds in a reverse process when the oxygen ions are eliminated under reverse bias.[23] In addition, Sample A with a relatively low sp^2 bonds content caused by the higher oxygen pressure exhibited a higher V_f. It seems to be owing to the inherent requirement of a higher electric field which is associated with more oxygen ion drifts necessary for the CF formation. Figure 1c plots the Cu layer thickness-dependent forming voltages of Sample B, depending on the Cu thickness. Forming-free-like behaviors were observed (Figure 1b). Thus, suitable use of stacked Cu layers in Sample B allows for gradual reduction in V_f up to 5 nm and then finally permits forming-free characteristics to take places. More detailed

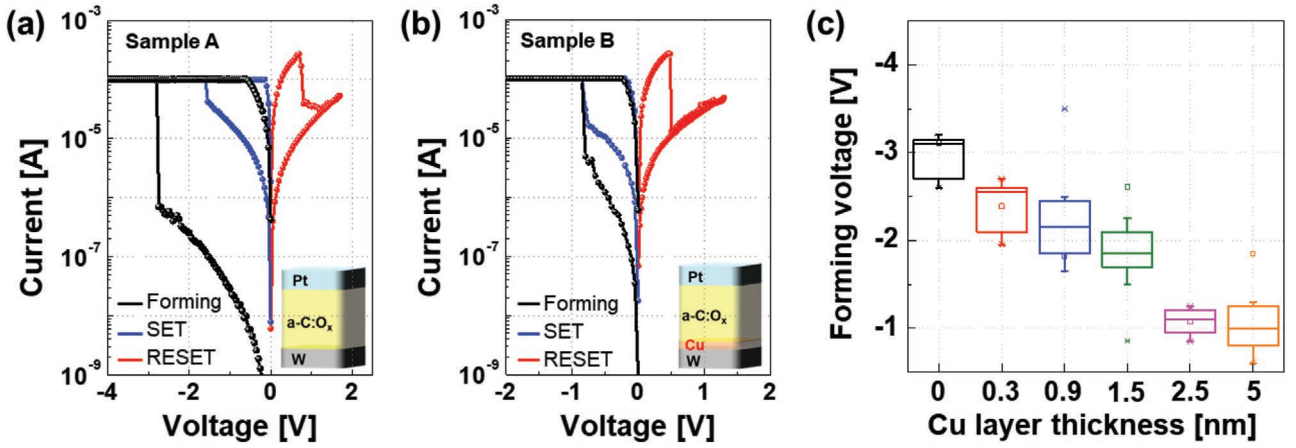

Figure 1. Representative *I*–*V* characteristics of Samples A and B exhibiting typical bipolar resistive switching behaviors. *I*–*V* responses of a) Sample A and b) Sample B, where Sample B reveals the forming-free feature through insertion of a suitable 2.5 nm thick Cu layer. Insets of panels (a) and (b) show the geometric layouts of Samples A and B, respectively. c) Cu thickness-dependence of forming voltages for Sample B, along with that of Sample A (black dot) for comparison.

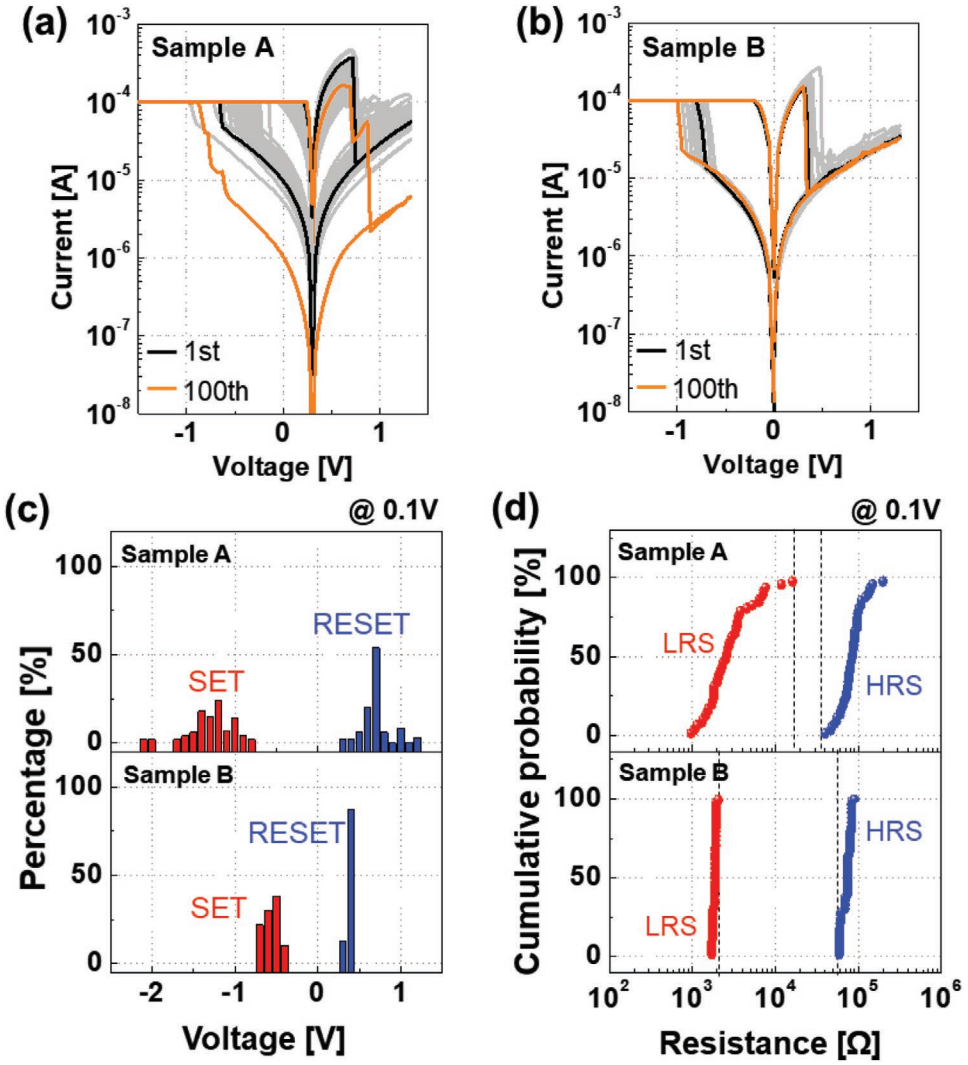

Figure 2. Representative DC endurance tests of a) Sample A and b) Sample B for 100 consecutive cycles. c) Set (red) and reset (blue) voltage distributions of Samples A and B during 100 consecutive DC cycles. d) Cumulative probability distributions of LRS (red) and HRS (blue) for Samples A and B taken at a real voltage of 0.1 V. Sample B identified the more stable electrical performance than that of Sample A.

I–V responses of Sample B with various Cu thicknesses are given in Figure S3 in the Supporting Information.

Figure 2 shows the representative *I–V* responses of Samples A and B taken as DC endurance tests. As seen in this figure, Sample A displayed undesirable *I–V* fluctuations even for 100 consecutive DC cycles (Figure 2a), while Sample B exhibited relatively stable *I–V* responses during the same 100 cycles (Figure 2b) by a simple stacked Cu layer. More additional *I–V* responses of Sample B for the test of device uniformity are given in Figure S4 in the Supporting Information. In particular, Sample A exhibited abnormally large fluctuations in a high resistance state (HRS) after 100 switching cycles. This unstable fluctuation mainly arises from the presence of unintended large CF gaps during repeated reset processes;[28] that is, random or nonuniform rupture and formation in the CFs occur, thereby providing unstable *I–V* characteristics when a suitable Cu layer is not used. The set and reset voltage distributions for Samples A and B during 100 consecutive DC cycles are given in Figure 2c, along with the thickness of α-C:O_x layer-dependent *I–V* response of Sample B (Figure S5, Supporting Information). Sample B exhibited a relatively stable set voltage (V_{set}) distribution in the range of –0.4 to –0.7 V, while Sample A displayed a wider range distribution from –0.8 to –2.1 V. Similarly, Sample B led to the improved reset voltage (V_{reset}) distribution from 0.3 to 0.5 V compared to that of Sample A in the range of 0.3 to 1.2 V. Figure 2d plots the cumulative probability distributions of LRS (red) and HRS (blue) for Samples A and B, respectively, where the measurements were taken at a real voltage of 0.1 V. The experimental findings suggest that suitable integration of the Cu layer in Sample B also enhances the stability for LRS and HRS, which will be described in more detail later. In addition, a detailed *I–V* response of Samples A and B with a 720 nm diameter is also given in Figure S6 in the Supporting Information for comparison, where particular measurement was carried out under a relatively higher compliance current of 10 mA.

To clarify the difference in device performance for Samples A and B, the composition and chemical bonding states of Samples A and B were carefully examined via XPS depth profile

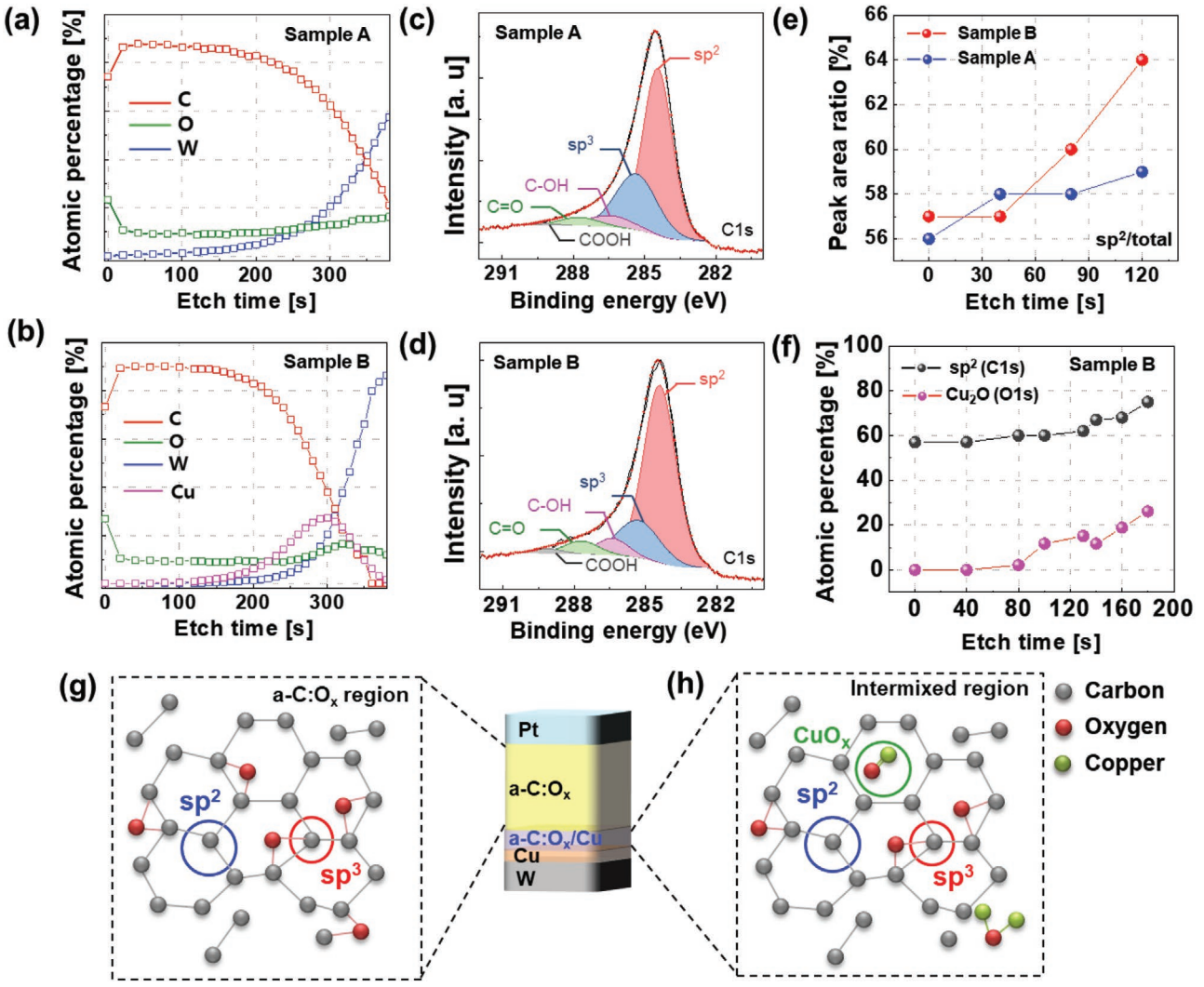

Figure 3. XPS depth profile spectra of C, O, W, and Cu observed from a) Sample A and b) Sample B. XPS spectra of C 1s core levels for c) Sample A and d) Sample B taken at the α-C:O_x/Cu interfaces after the etching time of 150 s. e) Summarized peak area ratios of sp^2 to the total areas for Samples A and B acquired at various in situ etching times ranging from 0, 40, 80, and 120 s. The plot of Sample B revealed an obvious increase in sp^2 ratio with increasing etching times. f) XPS spectra of C Is and O 1s core levels at the α-C:O_x/Cu interfaces of Sample B versus sputtering etching time. Possible chemical bonding schematics of Sample B at g) the α-C:O_x active region and h) intermixed regions of α-C:O_x/Cu interfaces, where the intermixed regions provided more sp^2 bonds due to the presence of C—O bonds.

measurements. **Figure 3**a,b shows the XPS depth profiles of Samples A and B, respectively, depending on the Ar ion etching time. As evident, the Cu peak in Sample B after an etching time of 150 s implies the presence of an intermixed region at the α-C:O_x/Cu interfaces. More detailed C 1s XPS spectra of Samples A and B monitored at an etching time of 150 s are provided in Figure 3c,d. The C 1s core-level spectra observed from Samples A and B were identified by the sp^2 (284.4 eV), sp^3 (285.3 eV) and C–O groups, which were composed of C–OH, C=O, and COOH at 286.4, 287.7, and 289 eV, respectively.[29–31] In Sample B, stacking a proper Cu layer reflects an increase in intensity of sp^2 bonds higher than that of Sample A. Figure S7 in the Supporting Information shows the XPS spectra of O 1s and Cu $2p_{3/2}$. The O 1s spectra of Sample A presented only two dominant peaks of C–O/C=O at 533.4 and 531.7 eV, respectively. Sample B provided three dominant peaks: the same C–O/C=O peaks as in Sample A and an additional Cu—O bond peak at 530.6 eV.[32] The de-convolution of the Cu $2p_{3/2}$ spectrum for Sample B provided two main peaks at 932.4 and 933.6 eV, indicating the presence of Cu^+ and Cu^{2+}, respectively.[33] However, Sample A exhibited no Cu $2p_{3/2}$ spectrum since no Cu layer was used. Figure 3e shows the peak area ratios of sp^2 to the total area for Samples A (blue) and B (red) acquired at various in situ etching times of 0, 40, 80, and 120 s. As seen in this figure, Sample B revealed an obvious increase in the peak area ratios of sp^2 with increasing etching time when a 2.5 thick Cu layer was adapted. Figure 3f plots the atomic percentage of sp^2 and Cu_2O for Sample B versus the sputtering etching time. The results also support the presence of the intermixed regions described above. These XPS analyses imply that stacking a suitable Cu layer may provide additional sp^2 content at the intermixed regions via the presence of Cu—O bonds, which are inevitably created during sputtering in the reaction

process between oxygen and carbon ions. Thus, the thickness of a Cu stacked layer seems to impact the proportion of sp^2 bonds in intermixed region through the formation of Cu—O bonds and a decrease in sp^3 bonds. Figure 3g,h illustrates the sp^2 and sp^3 bonds in the α-C:O_x bulk and intermixed regions, respectively, where the presence of additional Cu—O bonds is shown in Figure 3h, along with the representative sp^3 and sp^2 bonds. As plotted in Figures S1e and S2 in the Supporting Information, forming voltages increased from –1 to –3.5 V with decreasing sp^2 bonds, which means that the forming voltage is strongly affected by the sp^2 bonds at the α-C:O_x layer. It is worth noting that the XPS measurements for Sample B identify the appearance of more sp^2 bonds in the intermixed regions. These results reflect a higher possibility of establishing thick CFs via more sp^2 bonds even at a low operating voltage, thereby leading to a forming-free *I–V* response. In addition, the appearance of additional Cu—O bonds has a significant impact on reliability characteristics.

To examine the RS nature for Sample B at pristine, SET, and RESET states, the oxygen and Cu distribution in the SET/RESET states were carefully monitored because the elemental line profiles of TEM images at each state provide indirect information on the switching nature. In these TEM analyses, the other Pt/α-C:O_x(70)/Cu(2.5)/W stacks with a crossbar configuration and relatively thick active layer were prepared, which was denoted as Sample C for convenience. More detailed *I–V* responses of Sample C with/without having a Cu-stacked layer is given in Figure S8 in the Supporting Information. As seen, the results of Sample C exhibited the similar *I–V* responses to the behaviors of Sample B. The Sample C also confirmed the forming free characteristics, which are similar to those of Sample B. This was the main reason why we have chosen a relatively 70 nm thick active layer for the TEM analyses. **Figure 4**a shows a crosspoint geometric sketch and its enlarged cross-sectional picture of Sample C. Figure 4b displays the cross-sectional TEM images exhibiting the uniform growth of each layer, where a closer investigation identifies the appearance of the intermixed regions (yellow box). Figure 4c plots the elemental line profiles of Pt, W, O, C, and Cu of Sample C. In a pristine state, the carbon and oxygen elements were well-uniformly distributed over the whole α-C:O_x active region and extended to the top region of the W bottom electrode. After the SET operation, a clear increase in oxygen ions at the intermixed region and Cu layer reflects the bias-dependent oxygen ion drift. Their results support an increase in sp^2 bonds at the SET state, thereby establishing the CFs. During the RESET operation, the oxygen ions return back toward the α-C:O_x active regions, indicating a reduction in sp^2 bond content at the intermixed regions. This results in rupture events of the CFs, thus staying in HRS. Thus, the number and thickness of C—C sp^2 bonds can be reduced or ruptured by the oxygen ions accumulated under negative bias; that is, the release and accumulation

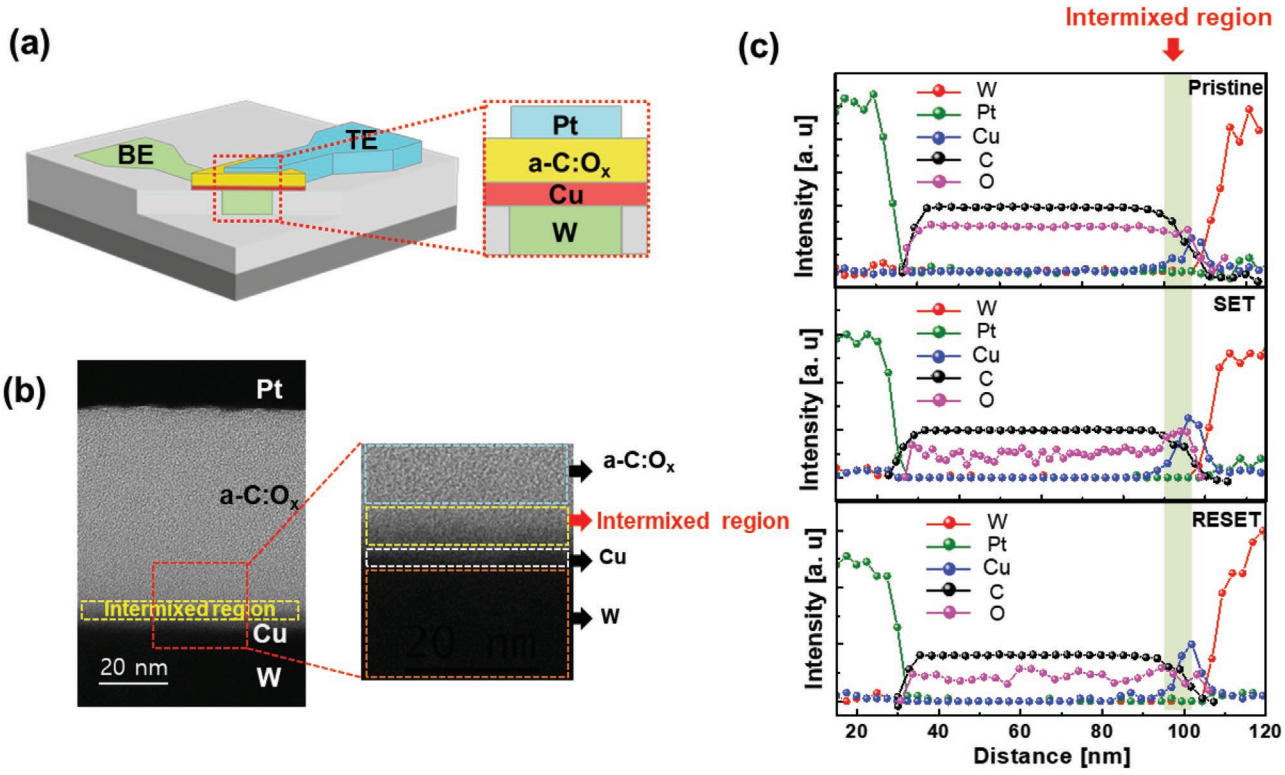

Figure 4. a) Schematic views of Sample C with a 30×30 μm^2 cell area, which were prepared for efficient TEM analyses. b) Cross-sectional TEM images of Sample C exhibiting the presence of the intermixed regions (yellow box) of α-C:O_x/Cu interfaces. c) Plots of EELS line profiles (O, C) and EDS line profiles (Cu, W, and Pt) taken at the pristine (top), set (middle), and reset (bottom) states, respectively. The pristine state exhibited uniformly distributed oxygen and carbon elements at the α-C:O_x active region. The SET operation reflected an increase in oxygen ions at the intermixed regions and Cu layer, while the copper element remains nearly unaffected. The RESET operation caused oxygen ions to drift back toward the α-C:O_x active regions, without experiencing distinct variation in Cu. The experimental findings verify indirect evidence for the formation of oxygen ion drift-driven sp^2 conductive filament, which is highly linked with the RS behavior.

of oxygen ions at intermixed regions are expected to chemically help the rupture and generation of the conductive carbon paths, which is called as predominantly electrochemical redox reaction of carbon complex through assistance of oxygen ion drifts. However, a more close analysis of Cu elements indicated that the Cu elements remained nearly unaffected during the SET and RESET operations. Thus, the dominant or main RS switching nature of Sample B may be described by the rupture and formation events of sp^2 bond CFs in the intermixed region, even though partial or less contribution of electrochemical memory effect (ECM) caused by the previously well-known Cu filaments to the RS event is also possible. In addition, we can exclude the possibility of oxygen vacancy contribution on the formation of conductive filaments mainly observed from various oxide-based RS. Previously representative work by other group[23] reported the switching nature arising from both hydrogenated amorphous carbon (α-C:H) and α-C:O_x active layers for comparison. Their *I*–*V* responses indicated that the conductive paths of both α-C:H and α-C:O_x devices mainly comes from the carbon. Thus, we anticipate that the release and accumulation of oxygen ions at intermixed regions could chemically help the rupture and generation of the conductive carbon paths, even though the conductive paths contributed by oxygen ions may partially take places.

To provide indirect evidence concerning sp^2 bond CFs, plots of the temperature-dependent LRS resistance for Samples A and B are given in Figure S9 in the Supporting Information. This measurement estimates the thermally activated electrical transport characteristics, which indicate whether the RS relies on the rupture and formation of Cu metallic filaments frequently extracted from the previous RS devices.[34–36] For example, it is widely believed that increasing LRS resistance with increasing temperatures reflects the presence of Cu metallic CFs in the case of the ECM process. But, as seen in plots of Figure S9a,b in the Supporting Information, both samples exhibited a decrease in LRS with increasing temperatures in the range of 300 to 450 K. These results support that the possible dominant RS behavior for both samples is mainly the consequence of sp^2 bond CFs via the electrochemical redox reaction upon bias. In addition, the possibility of interface effect on resistive switching nature was excluded owing to the following reasons: One is due to the higher electron affinity of carbon, where the carbon does not oxidize easily: that is in α-C:O_x memory device, a higher electron affinity of carbon likely may contribute to the possibility of excluding the carbon oxidation event at interfaces since the carbon/metal electrode interface does not serve as oxygen reservoir, thereby providing no oxidation reaction process at interfaces. This was one reason for the exclusion of interface effect in our work, even though any complex reaction process at interfaces may probably occur. The other evidence is the independent *I*–*V* features of samples with different diameter sizes of 340 and 720 nm, thereby ensuring the filamentary-type resistive switching nature (Figure S10, Supporting Information).

With the above observations, a more detailed RS nature of Samples A and B is proposed in **Figure 5**. In Sample A, the initial state before electroforming has randomly distributed oxygen ions over the whole α-C:O_x active layer (Figure 5a).

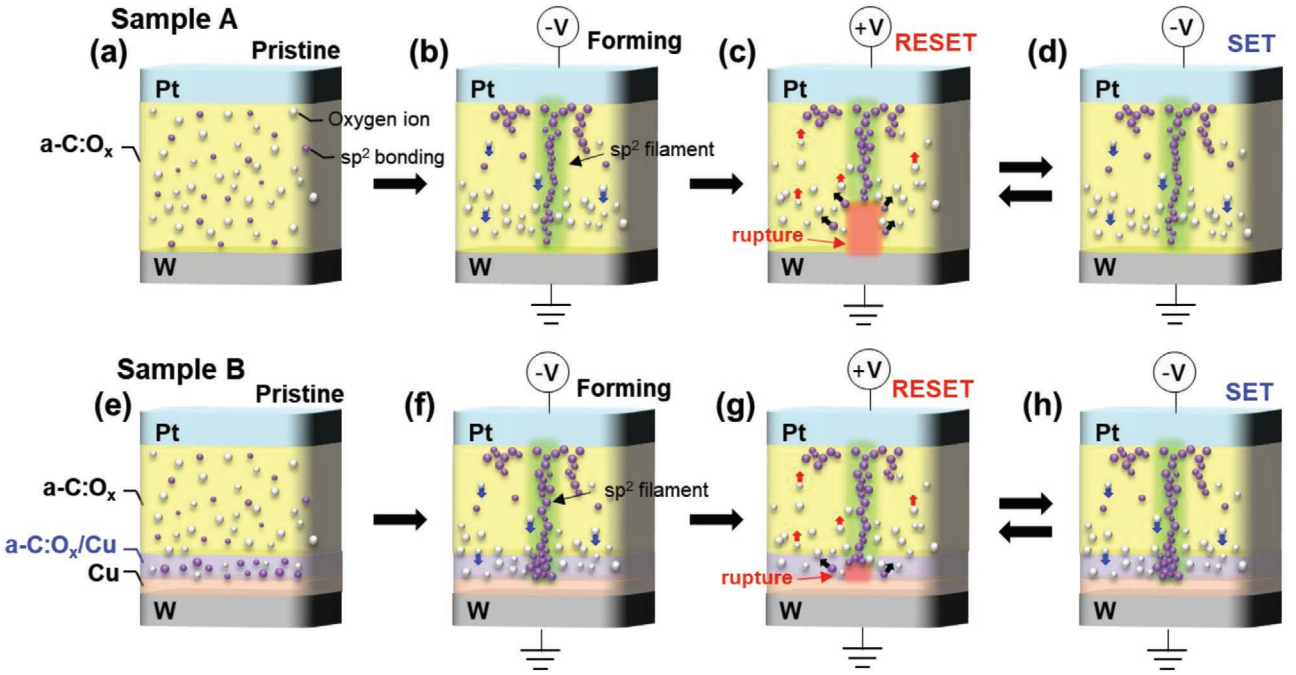

Figure 5. Possible resistive switching models for Samples A and B. a–d) Schematic oxygen ion-migration-dominated switching kinetics of Sample A. a) Pristine state containing randomly distributed oxygen ions. b) Forming process causing oxygen ion movement toward the bottom electrode followed by the formation of the CF by sp^2 bonds under a negative bias. c) RESET process under a positive voltage, creating random rupture events of CFs in a relatively wide region. d) SET process forming a full CF path. e–h) Schematic oxygen ion-drift-driven switching kinetics of Sample B. e) Pristine state including an additional increase in sp^2 bond content at the intermixed region of α-C:O_x/Cu interfaces. f) Forming process causing oxygen ion movement toward the Cu layer. g) RESET process leading to the main rupture events of CFs in the intermixed region. h) SET process generating the full CF paths, where relatively thick CFs at the intermixed region are expected, owing to the presence of more sp^2 bonds.

The results indicate that the resistances are primarily governed by the bulk properties of α-C:O_x active layer. Upon a negative forming voltage, oxygen ions drift toward the W bottom electrode (Figure 5b), resulting in the formation of CFs. The oxygen ion drift causes the formation of CFs from the upper Pt electrode. Under the RESET process, the existing CFs randomly ruptured in the wide regions (Figure 5c), thus providing device instability. Application of a negative voltage (SET process) allows for oxygen ion drift toward the W bottom electrode (Figure 5d), thus leading to the LRS. In Sample B, the initial state also has randomly distributed oxygen ions over the α-C:O_x active layer, except for an additional increase in sp^2 bonds at the intermixed region (Figure 5e). More sp^2 bonds appear in the intermixed regions due to the presence of the Cu—O bonds created by a stacked Cu layer, thus providing the relatively thick CFs (Figure 5f). When the top electrode is negatively biased, the oxygen ions drift toward the Cu layer and accumulated at the intermixed region. The positive bias (RESET process) permits the accumulated oxygen ions to move away from the intermixed regions, thus creating ruptured CFs in the intermixed regions (Figure 5g). Afterward, applying a negative voltage also enables the accumulation of oxygen ions at the intermixed regions again, thereby generating thick CFs (Figure 5h). The possible presence of relatively thicker filaments by sp^2 bonds in Sample B means an increase in the number of carbon bonds constituting of the filaments, compared with those of Sample A. In addition, the appearance of thicker filaments in Sample B may suggest a possible suppression in the number of the generated filaments with respect to the given sample area, thereby enabling decrease in the randomness of Sample B, compared with that of Sample A. Thus, all of the above reasons seem to result in the stable RS phenomena in Sample B.

In addition, to predict possible contribution of a Joule heating effect under bias to the RS nature of Sample B, the thermal conductivity (k) of each material was considered. Previous works found the k values of Cu—O bonds and α-C to be 33 and 0.01 W m^{-1} K^{-1}, respectively.[37] However, the thermal conductivity of α-C:O_x was not clearly identified because research on this material was in the early stages. However, such carbon-based materials are expected to have a low thermal conductivity. Therefore, it is predicted that the k value of Cu—O bonds is greater than that of C—O. The higher k of Cu—O bonds suggests the possibility of excluding the Joule heating effect in Sample B because of rapid thermal energy transfer from the intermixed regions toward neighboring active regions; that is, the dominant nature of Sample B is primarily associated with sp^2/sp^3 conversion at the intermixed regions, while a possible joule heating effect has less contribution to the RS behaviors of the whole operating process. In particular, the presence of Cu—O bonds at the intermixing region is likely attributed to reduction in random formation and rupture of the conductive paths by the sp^2 bond because the sp^2/sp^3 conversion arises mainly from electric field contribution, along with extremely small contribution of Joule heating.

Figure 6 shows the representative retention and endurance characteristics of LRS and HRS for Samples A and B, where the

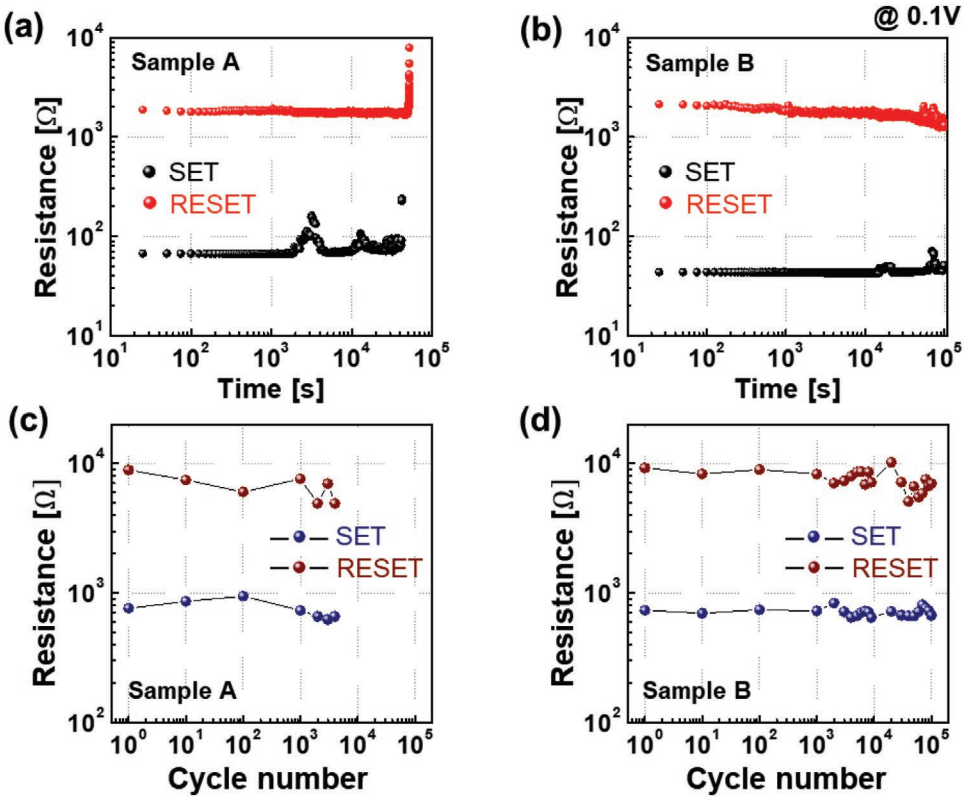

Figure 6. Switching reliability analyses of Samples A and B. Retention characteristics of a) Sample A and b) Sample B taken at a read voltage of 0.1 V, ensuring improved characteristics of Sample B up to 10^5 s. AC endurance features of c) Sample A and d) Sample B, where Sample B displayed relatively stable electric characteristics for 10^5 cycles.

measurements were taken at a reading voltage of 0.1 V at room temperature. In Sample A, the HRS resistance was observed for a period of 5×10^4 s, while the LRS resistance was held for 4×10^4 s (Figure 6a). Sample B led to enhanced LRS and HRS resistances up to 10^5 s (Figure 6b). More detailed retention characteristics of Samples A and B monitored at 85 °C serving as one of harsh condition are given in Figure S11 in the Supporting Information. Similarly, pulse endurance measurements were conducted (Figure 6c,d), where the data were monitored at 0.1 V during repeated switching between the LRS and HRS. Sample B revealed more stable switching behaviors during 10^5 pulse cycles than that of Sample A. To further validate the usefulness of Sample B, the pulse switching responses of Sample B at the Forming, SET, and RESET states were recorded (Figure S13, Supporting Information), in which triangular pulse shapes were employed. The corresponding voltages of the Forming, SET, and RESET states appeared at 1.6, 1.3, and 1.6 V, respectively (Figure S13a–c, Supporting Information). These results are comparable to the voltages taken from the DC analyses. Figure S13d,e in the Supporting Information plots the square pulse shape responses of Sample B in the SET and RESET states to identify their switching speeds. The corresponding switching speeds of the SET and RESET states were around 30 and 20 ns, respectively, which were comparable to those found in other works[38,39] without undergoing device degradation via the stacked Cu layer. Detailed pulse characteristics of Sample A are also given for comparison in Figure S14 in the Supporting Information.

3. Conclusions

In summary, we introduced a simple approach to enhance device performance by stacking a suitable Cu layer on the Pt/α-C:O_x/W frame. The structural and electrical observations indicate that the intermixed region of the α-C:O_x/Cu interfaces by a stacked Cu layer seems to be essential to forming-free and stable device characteristics; that is, the intermixed region has the additional Cu—O bonds, resulting in increase in sp^2 bond CFs, as confirmed from the XPS analyses. Thus, the presence of these Cu—O bonds is likely attributable to reduction in random formation and rupture of sp^2 bond CFs, thus contributing to the improved stability. Thus, we anticipate that the suitable use of stacked Cu on carbon oxide-based RS devices might lead to progress toward the enhancement of device performance, even though more experiments must be conducted.

4. Experimental Section

Growth of α-C:O_x by Off-Axis Sputtering: In general, direct growth of the α-C:O_x active layer via conventional sputtering systems has the disadvantage of introducing the oxygen plasma etching issue during the growth. This phenomenon seems to be the consequence of the active reaction between O_2 plasma and carbon ions. This in turn produces carbon dioxide (CO_2) or carbon monoxide (CO) gas, which can easily disappear during sputtering. To overcome this issue, an off-axis sputtering technique was employed to avoid direct reactions between reactive species such as oxygen and carbon ions in the work. Preparation of the α-C:O_x layer was conducted via DC magnetron off-axis sputtering using a graphitic carbon target at a DC plasma power of 120 W, where the base and working pressures were 1×10^{-7} and 3×10^{-3} Torr under an Ar/O_2 gas mixture ambient, respectively. To determine the oxygen content-dependent device performance, the oxygen partial pressure (P_{O2}) was varied from 0% (amorphous carbon layer) to 7% at a fixed total pressure of 3 mTorr. For the XPS analyses, the α-C:O_x layer of 20–30 nm thickness was prepared on the bare Si wafer at different P_{O2}. In general, the amorphous pure carbon layer created by a graphite target only with Ar gas produced the conductive sp^2 bonds, while the use of additional oxygen plasma during growth of α-C:O_x generated both sp^2/sp^3 bonds, as seen in Figure S1 in the Supporting Information.

Device Fabrication: For electrical analyses, two set of samples were prepared on the micro/nanosized W bottom electrodes predetermined on the Si_3N_4 substrates to define the device active areas for comparison. In addition, a particular crosspoint configuration was adapted for the TEM analyses by employing a conventional optical lithography process.

Chemical and Electrical Characterization: Chemical bonding and component distribution of the pristine, SET, and RESET states were determined via XPS measurements using K-Alpha+ and STEM-EDS/EELS. DC and pulse *I–V* characteristics of devices were determined at room temperature using a Keithley 4200 semiconductor parameter analyzer (Keithley 4200 SPA, Keithley Instrument, Inc.).

Supporting Information

Supporting Information is available from the Wiley Online Library or from the author.

Acknowledgements

This research was in part supported by the MOTIE (Ministry of Trade, Industry & Energy (Grant No. 10068055) and by the Nano-Material Technology Development Program through the National Research Foundation of Korea (NRF) funded by the Ministry of Science and ICT (NRF-2021M3F3A2A0103775011 and NRF-2019M3F3A1A0307942213).

Conflict of Interest

The authors declare no conflict of interest.

Data Availability Statement

Research data are not shared.

Keywords

α-C:O_x active layer, Cu stacked layer, forming-free response, off-axis sputtering, sp^2 bond conductive filaments

Received: June 29, 2021
Revised: August 28, 2021
Published online: November 11, 2021

[1] F. Pan, S. Gao, C. Chen, C. Song, F. Zeng, *Mater. Sci Eng. R. Rep.* **2014**, *83*, 1.
[2] S. Slesazeck, T. Mikolajick, *Nanotechnology* **2019**, *30*, 352003.
[3] D. Ielmini, *Semicond. Sci. Technol.* **2016**, *31*, 063002.
[4] I. Valov, R. Waser, J. R. Jameson, M. N. Kozicki, *Nanotechnology* **2011**, *22*, 254003.
[5] C. Ye, J. Wu, G. He, J. Zhang, T. Deng, P. He, H. Wang, *J. Mater. Sci. Technol.* **2016**, *32*, 1.

[6] W. Sun, B. Gao, M. Chi, Q. Xia, J. J. Yang, H. Qian, H. Wu, *Nat. Commun.* **2019**, *10*, 3453.
[7] R. Waser, R. Dittmann, G. Staikov, K. Szot, *Adv. Mater.* **2009**, *21*, 2632.
[8] M. Lanza, H. S. P. Wong, E. Pop, D. Ielmini, D. Strukov, B. C. Regan, L. Larcher, M. A. Villena, J. J. Yang, L. Goux, *Adv. Electron. Mater.* **2019**, *5*, 1800143.
[9] J. J. Yang, F. Miao, M. D. Pickett, D. A. Ohlberg, D. R. Stewart, C. N. Lau, R. S. Williams, *Nanotechnology* **2009**, *20*, 215201.
[10] G. Khurana, N. Kumar, M. Chhowalla, J. F. Scott, R. S. Katiyar, *Sci. Rep.* **2019**, *9*, 15103.
[11] A. Sebastian, A. Pauza, C. Rossel, R. M. Shelby, A. F. Rodríguez, H. Pozidis, E. Eleftheriou, *New J. Phys.* **2011**, *13*, 013020.
[12] T. J. Raeber, Z. C. Zhao, B. J. Murdoch, D. R. McKenzie, D. G. McCulloch, J. G. Partridge, *Carbon* **2018**, *136*, 280.
[13] S. Qin, J. Zhang, D. Fu, D. Xie, Y. Wang, H. Qian, L. Liu, Z. Yu, *Nanoscale* **2012**, *4*, 6658.
[14] A. Ott, C. Dou, U. Sassi, I. Goykhman, D. Yoon, J. Wu, A. Lombardo, A. Ferrari, *2D Mater.* **2018**, *5*, 045028.
[15] E. Gerstner, D. McKenzie, *J. Appl. Phys.* **1998**, *84*, 5647.
[16] D. Fu, D. Xie, T. Feng, C. Zhang, J. Niu, H. Qian, L. Liu, *IEEE Electron Device Lett.* **2011**, *32*, 803.
[17] J. Xu, D. Xie, T. Feng, C. Zhang, X. Zhang, P. Peng, D. Fu, H. Qian, T.-l. Ren, L. Liu, *Carbon* **2014**, *75*, 255.
[18] P. Peng, D. Xie, Y. Yang, C. Zhou, S. Ma, T. Feng, H. Tian, T. Ren, *J. Phys. D: Appl. Phys.* **2012**, *45*, 365103.
[19] F. J. Romero, A. Toral, A. Medina-Rull, C. L. Moraila-Martinez, D. P. Morales, A. Ohata, A. Godoy, F. G. Ruiz, N. Rodriguez, *Front. Mater.* **2020**, *7*, 17.
[20] G. Khurana, P. Misra, R. S. Katiyar, *J. Appl. Phys.* **2013**, *114*, 124508.
[21] L.-H. Wang, W. Yang, Q.-Q. Sun, P. Zhou, H.-L. Lu, S.-J. Ding, D. W. Zhang, *Appl. Phys. Lett.* **2012**, *100*, 063509.
[22] Y. J. Chen, H. L. Chen, T. F. Young, T. C. Chang, T. M. Tsai, K. C. Chang, R. Zhang, K. H. Chen, J. C. Lou, T. J. Chu, J. H. Chen, D. H. Bao, S. M. Sze, *Nanoscale Res. Lett.* **2014**, *9*, 52.
[23] C. A. Santini, A. Sebastian, C. Marchiori, V. P. Jonnalagadda, L. Dellmann, W. W. Koelmans, M. D. Rossell, C. P. Rossel, E. Eleftheriou, *Nat. Commun.* **2015**, *6*, 8600.
[24] X.-C. Yuan, J.-L. Tang, H.-Z. Zeng, X.-H. Wei, *Nanoscale Res. Lett.* **2014**, *9*, 268.
[25] K. Skaja, M. Andrä, V. Rana, R. Waser, R. Dittmann, C. Baeumer, *Sci. Rep.* **2018**, *8*, 10861.
[26] C. Baeumer, R. Valenta, C. Schmitz, A. Locatelli, T. O. Menteş, S. P. Rogers, A. Sala, N. Raab, S. Nemsak, M. Shim, *ACS Nano* **2017**, *11*, 6921.
[27] Z. Wei, Y. Kanzawa, K. Arita, Y. Katoh, K. Kawai, S. Muraoka, S. Mitani, S. Fujii, K. Katayama, M. Iijima, *IEEE Int. Electron Devices Meet., Tech. Dig.* **2008**, *293*, 5671467.
[28] C. Wang, H. Wu, B. Gao, T. Zhang, Y. Yang, H. Qian, *Microelectron. Eng.* **2018**, *187*, 121.
[29] B.-J. Kim, J.-P. Kim, J.-S. Park, *Nanoscale Res. Lett.* **2014**, *9*, 236.
[30] M. Jin, H.-K. Jeong, T.-H. Kim, K. P. So, Y. Cui, W. J. Yu, E. J. Ra, Y. H. Lee, *J. Phys. D: Appl. Phys.* **2010**, *43*, 275402.
[31] L. Chen, Z. Xu, J. Li, B. Zhou, M. Shan, Y. Li, L. Liu, B. Li, J. Niu, *RSC Adv.* **2014**, *4*, 1025.
[32] Q. Wang, T. Li, P. Xie, J. Ma, *J. Environ. Chem. Eng.* **2017**, *5*, 2648.
[33] B. Chen, R. Xu, R. Zhang, N. Liu, *Environ. Sci. Technol.* **2014**, *48*, 13909.
[34] S. Gao, C. Song, C. Chen, F. Zeng, F. Pan, *J. Phys. Chem. C* **2012**, *116*, 17955.
[35] F. Zhuge, S. Peng, C. He, X. Zhu, X. Chen, Y. Liu, R.-W. Li, *Nanotechnology* **2011**, *22*, 275204.
[36] T. Tan, T. Guo, Z. Wu, Z. Liu, *Chin. Phys. B* **2016**, *25*, 117306.
[37] A. A. Balandin, *Nat. Mater.* **2011**, *10*, 569.
[38] R. Cao, S. Liu, Q. Liu, X. Zhao, W. Wang, X. Zhang, F. Wu, Q. Wu, Y. Wang, H. Lv, *IEEE Electron Device Lett.* **2017**, *38*, 1371.
[39] C.-Y. Lin, P.-H. Chen, T.-C. Chang, K.-C. Chang, S.-D. Zhang, T.-M. Tsai, C.-H. Pan, M.-C. Chen, Y.-T. Su, Y.-T. Tseng, *Nanoscale* **2017**, *9*, 8586.